

# Finite size scaling of survival statistics in metapopulation models

Alice Doimo,<sup>1,2</sup> Giorgio Nicoletti,<sup>3</sup> Davide Bernardi,<sup>1,2</sup> and Prajwal Padmanabha<sup>4</sup>

<sup>1</sup>*Laboratory of Interdisciplinary Physics, Department of Physics and Astronomy “G. Galilei”, University of Padova, Via Marzolo 8, 35131 Padova, Italy*

<sup>2</sup>*National Biodiversity Future Center, Piazza Marina 61, 90133, Palermo, Italy*

<sup>3</sup>*Laboratory of Ecohydrology, School of Architecture, Civil and Environmental Engineering, École Polytechnique Fédérale de Lausanne, Lausanne 1015, Switzerland*

<sup>4</sup>*Department of Fundamental Microbiology, University of Lausanne, Switzerland*

Spatial metapopulation models are fundamental to theoretical ecology, enabling to study how landscape structure influences global species dynamics. Traditional models, including recent generalizations, often rely on the deterministic limit of stochastic processes, assuming large population sizes. However, stochasticity - arising from dispersal events and population fluctuations - profoundly shapes ecological dynamics. In this work, we extend the classical metapopulation framework to account for finite populations, examining the impact of stochasticity on species persistence and dynamics. Specifically, we analyze how the limited capacity of local habitats influences survival, deriving analytical expressions for the finite-size scaling of the survival probability near the critical transition between survival and extinction. Crucially, we demonstrate that the deterministic metapopulation capacity plays a fundamental role in the statistics of survival probability and extinction time moments. These results provide a robust foundation for integrating demographic stochasticity into classical metapopulation models and their extensions.

## I. INTRODUCTION

Understanding the dynamics of populations distributed across fragmented habitats is a longstanding challenge in ecology and conservation biology. Metapopulation theory provides a foundational framework for examining how local extinctions and landscape-mediated colonization processes shape the collective dynamics of spatially structured populations over time [1–10]. The concept of metapopulation, first introduced by Levins [11], describes a “population of populations”, i.e., a set of distinguished subpopulations that are spatially separated, but interconnected by the ongoing exchange of individuals. This exchange occurs across a spatial network of habitat patches, varying in quality, connectivity, and area [2]. Both field and theoretical studies have highlighted the validity of this approach, showing that landscape topology significantly influences the flow of individuals between habitats, ultimately determining the survival or extinction of the metapopulation [12–16].

In particular, to capture the effects of spatial structure and habitat fragmentation on species persistence, Hanski and Ovaskainen introduced a fundamental measure known as metapopulation capacity [17–19], which determines the survival of a focal species within a given landscape. This measure is defined as the maximum eigenvalue of an appropriate landscape matrix, and allows a direct comparison between theoretical models and real-world networks of habitat fragments [20]. The application of network theory to spatial ecology [21–23] has advanced the study of complex dispersal network structures [5, 24–28]. However, metapopulation capacity has traditionally been defined within deterministic models, which overlook fluctuations arising from demographic and environmental stochasticity [29–31]. Early contributions by Lande [32] and Hanski [33] pioneered the integration

of stochasticity into metapopulation dynamics, emphasizing the increased risk of extinction posed by random fluctuations at low population levels. Migration through spatially connected patches, by contrast, provides insurance against simultaneous global extinction, underscoring the fundamental role of dispersal network topology. Classical approaches to studying these dynamics, such as Stochastic Patch Occupancy Model [34, 35], the Incidence Function Model [33] and their extensions [36–39], have enabled the computation of extinction times and quasi-stationary occupancy distributions. However, these approaches predominantly rely on purely numerical methods due to the complexity of stochastic processes, spatial heterogeneity, and variability in the parameter space [40]. Consequently, in metapopulation dynamics, qualitative results are often obtained from deterministic approximations of stochastic processes, which lead to theoretically tractable models and provide broad qualitative insights [4].

In this work, we rigorously extend the traditional deterministic metapopulation framework by explicitly incorporating the stochasticity of individual-level processes to analytically investigate their potential impact on metapopulation dynamics and persistence. To incorporate stochasticity from the ground up, we focus on the role of finite carrying capacity, i.e., the maximum size of the subpopulations that compose the metapopulation. This approach offers a precise way to control fluctuations, allowing us to disentangle the effects of local demographic stochasticity and dispersal network topology. Specifically, we examine whether critical thresholds in carrying capacity exist beyond which stochastic fluctuations become catastrophic, or conversely, whether there are local system sizes beyond which population persistence is significantly enhanced. To address this question, we build upon our previous work, which extends the de-

terministic spatial metapopulation model developed by Hanski and Ovaskainen to arbitrary landscape structures [5]. We adopt a bottom-up approach, starting from a microscopic model describing colonization, extinction, and dispersal of a focal species at the individual level.

To analytically study the stochastic dynamics of the system, we perform a Van Kampen inverse system-size expansion of the corresponding master equation [41], selecting the inverse of the carrying capacity of the patches - i.e., the maximum local population size supported by each patch - as the expansion parameter. Since the resulting Fokker-Planck equation is too complicated to provide analytical insights, we introduce a series of simplifying hypotheses. Primarily, we assume translational invariance within a complete network and marginalize to capture the effective behavior of representative single-site variables. By imposing a separation of timescales [42] between dispersal and local processes, we derive an effective one-dimensional quasi-stationary (QSS) Langevin equation that accurately captures the overall metapopulation dynamics. In the deterministic limit, we recover the expected absorbing phase transition [43, 44] between extinction and survival regimes, as determined by the system's metapopulation capacity. Stochasticity, however, renders the survival regime metastable - a key result, that is especially relevant for systems with small carrying capacity. Moreover, the effective QSS equation enables us to analytically study the general scaling behavior of the survival probability in the vicinity of the extinction transition. We demonstrate that near this transition point, the survival probability for different carrying capacities exhibits a universal behavior consistent with finite-size scaling [45, 46]. Furthermore, we analytically derive the scaling of the first and second moments of extinction time with varying carrying capacity, showing that they similarly collapse to a universal form.

Through this analysis, we bridge results from the deterministic metapopulation framework with its stochastic counterpart. We demonstrate that the metapopulation capacity - a deterministic measure - still plays a crucial role in the statistics of survival probability and extinction time moments.

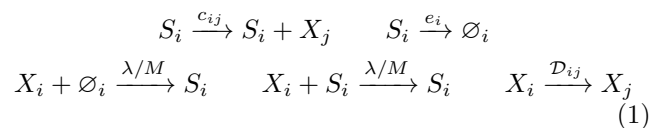
## II. MODEL

We introduce a model that describes the microscopic dynamics of a single species within a metapopulation. Individuals undergo processes such as birth, death, reproduction, and dispersal across a network of habitat patches. This model was proposed in [5], where the connection between its deterministic limit and the Hanski and Ovaskainen model [2, 18] was demonstrated. In this section, we first provide a detailed description of the microscopic processes governing the dynamics and then briefly recall the derivation of the macroscopic deterministic equations, as outlined in [5]. This is instrumental in the analysis of the full stochastic model, which we ana-

lyze in the following section.

### A. Microscopic ecological dynamics

We consider a dispersal network of  $N$  interconnected habitat patches, corresponding to the nodes of the dispersal network, inhabited by a given focal species. We separately model the behavior of two kinds of individuals: settled individuals (denoted by  $S$ ), which reside on the nodes of the network, and explorers ( $X$ ), which diffuse through the edges of the network. We denote the vector comprising all local abundances of individuals in each node by  $\vec{n} = (n_{X_1}, \dots, n_{X_N}; n_{S_1}, \dots, n_{S_N})$ , where  $n_{X_i}$  and  $n_{S_i}$  are the numbers of explorers and settled individuals in patch  $i$ , respectively. By assuming that each patch has a maximum carrying capacity of  $M$  settled individuals - i.e.,  $n_{S_i} + n_{\emptyset_i} = M \quad \forall i$ , where  $\emptyset_i$  denotes an empty site in patch  $i$  - we define the following microscopic reactions:



where the indices  $i, j = 1, \dots, N$  label the network patches. The rate  $e_i$  accounts for the death of a settled individual in patch  $i$ , while  $c_{ij}$  represents the rate at which an explorer in patch  $j$  is produced by a settled individual in a neighboring node  $i$ . An explorer in  $i$  can move to a connected patch  $j$  at rate  $\mathcal{D}_{ij}$  and may attempt to colonize one of the  $M$  sites at node  $j$  at a rate  $\lambda/M$ . The rescaling with  $M$  guarantees that the rate of colonization of a given patch does not depend on  $M$ . Colonization is successful if the patch has not reached maximum capacity; otherwise, the explorer dies. Diffusion rates are set in the form  $\mathcal{D}_{ij} = \mathcal{D} \mathcal{A}_{ij}$  with  $\mathcal{A}_{ij}$  the adjacency matrix of the dispersal network, denoting a possibly weighted connection between node  $j$  and node  $i$ . Similarly, the colonization rate  $c_{ij}$  is given by  $c_{ij} = c_i h(\mathcal{D}/\lambda) \mathcal{A}_{ij}$ , where  $h(f)$  is a function that encodes feasibility of exploration and  $f = \mathcal{D}/\lambda$  controls exploration efficiency. A Monod function  $h(f) = \frac{\xi_0}{1+1/f}$  is typically chosen to model the saturation effect of exploration feasibility, where  $\xi_0$  represents the maximal explorability.

### B. Deterministic equations

The deterministic equations resulting from the microscopic model defined in Eq. (1) are given by:

$$\begin{aligned} \dot{\rho}_i &= -e_i \rho_i + \lambda(1 - \rho_i) x_i & (2) \\ \dot{x}_i &= -\lambda x_i + h(f) \sum_{j=1}^N \mathcal{A}_{ji} c_j \rho_j + \mathcal{D} \sum_{j=1}^N (\mathcal{A}_{ji} x_j - \mathcal{A}_{ij} x_i) \end{aligned}$$

where  $\rho_i, x_i$  are the average population densities,  $\langle n_{S_i} \rangle / M$  and  $\langle n_{X_i} \rangle / M$ , respectively. In the limit in which

the explorers' dynamics is much faster than the dynamics of the settled population, one obtains an effective model describing the evolution of the settled population:

$$\dot{\rho}_i = -e_i \rho_i + (1 - \rho_i) \sum_{j=1}^N c_j K_{ji} \rho_j \quad (3)$$

where the kernel matrix  $K$  encodes the dependence of the population density on the topology of the dispersal network. We have that

$$K_{ji} = \sum_{k=1}^N C_{jk} F_{ik}^{-1} \quad (4)$$

where we introduced the matrix  $F = \mathbb{I} + fL^T$  that depends on the out-degree Laplacian of the network,  $L_{ij} = \delta_{ij} \sum_{k=1}^N A_{ik} - A_{ij}$ . The kernel matrix,  $K$ , introduces an effective coupling between settled populations residing in different patches. In particular, in [5] it was shown that

$$K_{ji} = h(f) \sum_{l=1}^N A_{jl} \sum_{k=1}^N \frac{V_{ik}(V^{-1})_{kl}}{1 + f\omega_k} \quad (5)$$

where  $\omega_k$  is the  $k$ -th eigenvalue of the transpose out-degree Laplacian of the dispersal network, and  $V_{ij} = v_i^{(j)}$  with  $\mathbf{v}^{(k)}$  the corresponding right eigenvector. Furthermore, from the deterministic model in Eq. (3), one can show that if  $e_i = e$  and  $c_i = c$  for all patches, the survival of the species is uniquely determined by the maximum eigenvalue of the dispersal kernel, i.e., the metapopulation capacity  $\lambda_M$  proposed by Hanski and Ovaskainen [17]. If  $\lambda_M > e/c$ , the species survives; otherwise, it goes extinct. A similar condition has been shown to hold when  $e_i$  explicitly depends on the patch index [27].

### III. STOCHASTIC MODEL

In deriving the deterministic dynamics given by Eq. (2), we have implicitly assumed a large carrying capacity, i.e.,  $M \rightarrow \infty$ . However, to investigate the effect of stochasticity on population persistence, we need to extend the deterministic model to account for finite carrying capacities, which introduce demographic fluctuations. For a

general model defined by a set of microscopic processes, the complete stochastic dynamics is governed by the master equation [47]

$$\partial_t \mathcal{P}(\vec{n}, t) = \sum_{\vec{n}' \neq \vec{n}} \left[ W(\vec{n}|\vec{n}') \mathcal{P}(\vec{n}', t) - W(\vec{n}'|\vec{n}) \mathcal{P}(\vec{n}, t) \right] \quad (6)$$

where  $\mathcal{P}(\vec{n}, t)$  is the probability that the system is in state  $\vec{n}$  at time  $t$ , and  $W(\vec{n}'|\vec{n})$  are the rates at which the system transitions from state  $\vec{n}$  to state  $\vec{n}'$ . The transition rates for our model can be straightforwardly derived from the reactions Eq. (1), leading to:

$$\begin{aligned} W(n_{S_i} - 1; n_{X_i} | n_{S_i}; n_{X_i}) &= e_i n_{S_i} \\ W(n_{S_i} + 1; n_{X_i} - 1 | n_{S_i}; n_{X_i}) &= \frac{\lambda}{M} n_{X_i} (M - n_{S_i}) \\ W(n_{S_i}; n_{X_i} - 1 | n_{S_i}; n_{X_i}) &= \frac{\lambda}{M} n_{X_i} n_{S_i} \\ W(n_{S_i}, n_{S_j}; n_{X_i} + 1, n_{X_j} | n_{S_i}, n_{S_j}; n_{X_i}, n_{X_j}) &= c_{ji} n_{S_j} \\ W(n_{S_i}, n_{S_j}; n_{X_i} + 1, n_{X_j} - 1 | n_{S_i}, n_{S_j}; n_{X_i}, n_{X_j}) &= \mathcal{D}_{ji} n_{X_j} \end{aligned} \quad (7)$$

where, for the sake of brevity, we explicitly write only the number of individuals at the nodes involved in the transition.

#### A. Fokker-Planck equation

Although no closed-form solution for the master equation of our model exists, the corresponding stochastic dynamics can be simulated exactly using the Gillespie algorithm [48]. We obtain analytical insight into the effects of stochasticity by means of a Van Kampen system size expansion [41, 49]. In particular, we take  $1/M$  as the natural expansion parameter, so that in the  $M \rightarrow \infty$  limit we recover the deterministic equations. To perform this expansion, it is convenient to rewrite the master equation in terms of step operators, defined by their action on a generic function  $f(\vec{n})$  as:

$$\xi_{A_i}^{\pm 1} f(n_{A_1}, \dots, n_{A_i}, \dots, n_{A_N}) = f(n_{A_1}, \dots, n_{A_i} \pm 1, \dots, n_{A_N}) \quad (8)$$

In terms of step operators, the master equation becomes:

$$\begin{aligned} \frac{\partial}{\partial t} \mathcal{P}(\vec{n}, t) &= \sum_{i=1}^N \left\{ \left[ (\xi_{S_i}^{+1} - 1) W(n_{S_i} - 1; n_{X_i} | n_{S_i}; n_{X_i}) + (\xi_{S_i}^{-1} \xi_{X_i}^{+1} - 1) W(n_{S_i} + 1; n_{X_i} - 1 | n_{S_i}; n_{X_i}) \right. \right. \\ &\quad \left. \left. + (\xi_{X_i}^{+1} - 1) W(n_{S_i}; n_{X_i} - 1 | n_{S_i}; n_{X_i}) \right] \mathcal{P}(n_{S_i}; n_{X_i}) \right\} \\ &\quad + \sum_{i=1}^N \sum_{j=1}^N \left\{ \left[ (\xi_{X_i}^{-1} - 1) W(n_{S_i}, n_{S_j}; n_{X_i} + 1, n_{X_j} | n_{S_i}, n_{S_j}; n_{X_i}, n_{X_j}) \right. \right. \\ &\quad \left. \left. + (\xi_{X_i}^{-1} \xi_{X_j}^{+1} - 1) W(n_{S_i}, n_{S_j}; n_{X_i} + 1, n_{X_j} - 1 | n_{S_i}, n_{S_j}; n_{X_i}, n_{X_j}) \right] \mathcal{P}(n_{S_i}, n_{S_j}; n_{X_i}, n_{X_j}) \right\}. \end{aligned} \quad (9)$$

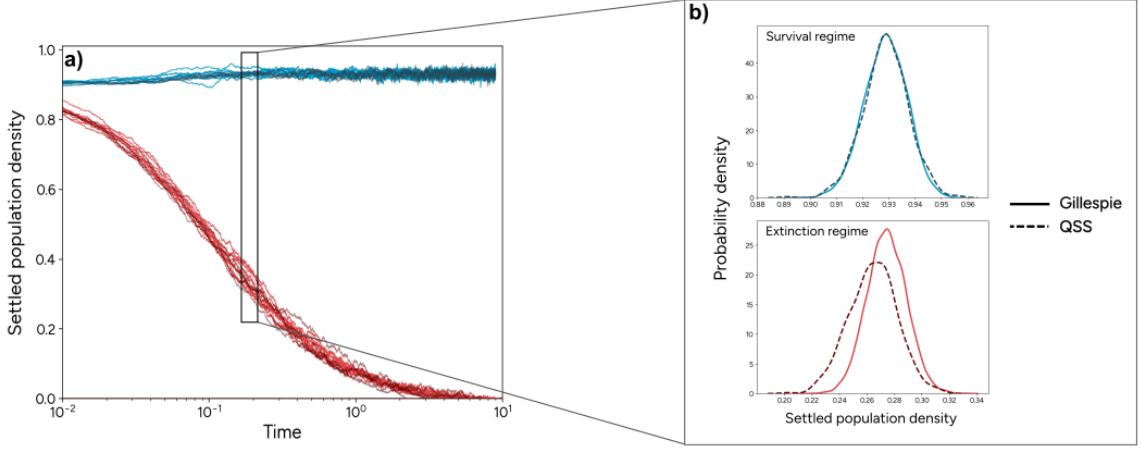


**FIG. 1.** Comparison between **a)** 5 realisations of the trajectories resulting from the mean-field quasi-stationary SDE Eq. (19) (integrated with the Euler-Maruyama method) and the Gillespie simulation reproducing the exact dynamics of the microscopic model Eq. (1). The parameters of the model are  $M = 1000$ ,  $N = 20$ ,  $f = 1$  which imply an effective metapopulation capacity of  $\lambda_M \sim 9.5$ . Survival regime ( $e/c < \lambda_M$ ):  $e = 10$ ,  $c = 1$ , extinction regime ( $e/c > \lambda_M$ ):  $e = 1$ ,  $c = 1.5$ .

If we define the population densities with respect to the system size parameter  $M$  as  $\rho_i = n_{S_i}/M$ ,  $x_i = n_{X_i}/M$ , the expansion of the master equation up to second order in powers of  $1/M$ , for fixed densities, yields the Fokker-Planck (FP) equation:

$$\begin{aligned} \partial_t \mathcal{P}(\vec{\rho}, \vec{x}, t) = & - \sum_{i=1}^N \partial_{\rho_i} [A_i^\rho(\vec{\rho}, \vec{x}) \mathcal{P}(\vec{\rho}, \vec{x}, t)] - \sum_{i=1}^N \partial_{x_i} [A_i^x(\vec{\rho}, \vec{x}) \mathcal{P}(\vec{\rho}, \vec{x}, t)] + \frac{1}{2} \sum_{i,j=1}^N \partial_{\rho_i} \partial_{\rho_j} [\mathbb{D}_{i,j}^{\rho\rho}(\vec{\rho}, \vec{x}) \mathcal{P}(\vec{\rho}, \vec{x}, t)] + \\ & + \frac{1}{2} \sum_{i,j=1}^N \partial_{x_i} \partial_{x_j} [\mathbb{D}_{i,j}^{xx}(\vec{\rho}, \vec{x}) \mathcal{P}(\vec{\rho}, \vec{x}, t)] + \sum_{i,j=1}^N \partial_{\rho_i} \partial_{x_j} [\mathbb{D}_{i,j}^{\rho x}(\vec{\rho}, \vec{x}) \mathcal{P}(\vec{\rho}, \vec{x}, t)]. \end{aligned} \quad (10)$$

Here the subscripts  $i, j, k$  label the network patches while the superscripts  $\rho, x$  refer to the settled and explorer population, respectively. The drift vector's components correspond to the deterministic model:

$$\begin{aligned} A_i^\rho &= \lambda x_i (1 - \rho_i) - e_i \rho_i \\ A_i^x &= \sum_j (\mathcal{D}_{j,i} x_j - \mathcal{D}_{i,j} x_i + c_{j,i} \rho_j) - \lambda x_i \end{aligned} \quad (11)$$

and the Fokker-Planck diffusion matrix has the following block structure

$$\mathbb{D} = \begin{pmatrix} \mathbb{D}^{\rho\rho} & \mathbb{D}^{\rho x} \\ \mathbb{D}^{x\rho} & \mathbb{D}^{xx} \end{pmatrix} \quad (12)$$

with blocks given by

$$\begin{aligned} \mathbb{D}_{ij}^{\rho\rho} &= \frac{1}{M} [e_i \rho_i + \lambda x_i (1 - \rho_i)] \delta_{ij} \\ \mathbb{D}_{ij}^{\rho x} &= \mathbb{D}_{ij}^{x\rho} = -\frac{1}{M} \lambda x_i (1 - \rho_i) \delta_{ij} \\ \mathbb{D}_{ij}^{xx} &= \frac{1}{M} \left[ \sum_k (\rho_k c_{ki} + x_i \mathcal{D}_{ik} + x_k \mathcal{D}_{ki}) + \lambda x_i \right] \delta_{ij} + \\ & - \frac{1}{M} (x_i \mathcal{D}_{ij} + x_j \mathcal{D}_{ji}) (1 - \delta_{ij}). \end{aligned} \quad (13)$$

where  $\delta_{ij}$  is the Kronecker delta. We highlight that all entries in the Fokker-Planck diffusion matrix are proportional to the inverse of the carrying capacity, explicitly showing that the leading order of the Van Kampen expansion yields the deterministic dynamics.

Although Eq. (10) provides an analytical description of our stochastic model in the limit of large system size  $M$ , a general analytical treatment remains cumbersome for large networks, as it would require tracking  $2N$  variables. Additionally, the explorers' noise strength,  $\mathbb{D}^{xx}$ , has non zero off-diagonal entries, coupling their dynamics across patches. Hence, we resort to a further simplification of Eq. (10) to enable a more direct understanding of the system's behavior.

## B. Effective SDE

To simplify the dynamics and reduce the number of variables, we assume a fully connected dispersal network  $\mathcal{A}_{ij} = \mathcal{A}(1 - \delta_{ij})$ , and homogeneous habitat patches  $c_i = c$ ,  $e_i = e \forall i$ , implying that the system is invariant under translations.  $\mathcal{A}$  is set to  $1/N$  to ensure a well-

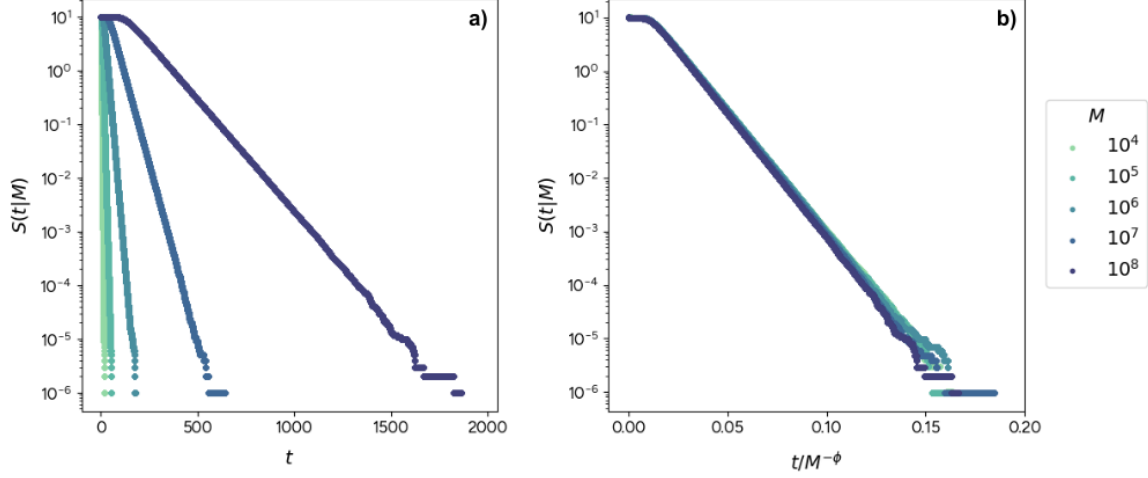


**FIG. 2.** Survival probability of the quasi-stationary SDE as a function of time  $t$  and system size  $M$ : (a) not rescaled. (b) rescaled according to Eq. (23), with the numerical estimates of the scaling given in Eq. (26). The system is set at criticality and the initial condition is fixed at  $\rho = \frac{1}{2}$ . The microscopic parameters of the model are  $N = 201$ ,  $\lambda = 100$ ,  $D = 100$ ,  $e/c = \lambda_M = 100$ . Averages are obtained over  $10^7$  numerical realizations of the dynamics in Eq. (19), using Euler-Maruyama algorithm.

defined limit for  $N \rightarrow \infty$ .

To gain analytical insight, we focus on the marginalized probability distribution, by integrating out all variables except those associated with a single site,  $(\rho_1, x_1) \equiv (\rho, x)$ :

$$\int \prod_{i \geq 2} [d\rho_i dx_i] \mathcal{P}(\vec{\rho}, \vec{x}, t) = P(\rho, x, t). \quad (14)$$

Motivated by our assumption of a fully connected dispersal network, we adopt the following approximation for each  $\rho_j, x_j$ :

$$\begin{aligned} \int \prod_{i \geq 2} [d\rho_i dx_i] \mathcal{P}(\vec{\rho}, \vec{x}, t) x_j &\approx P(\rho, x, t) x \\ \int \prod_{i \geq 2} [d\rho_i dx_i] \mathcal{P}(\vec{\rho}, \vec{x}, t) \rho_j &\approx P(\rho, x, t) \rho \end{aligned} \quad (15)$$

Finally, we take the limit  $N \rightarrow \infty$ , obtaining the simplified equation:

$$\begin{aligned} \frac{\partial}{\partial t} P(\rho, x, t) &= -\partial_\rho \{ [\lambda x (1 - \rho) - e \rho] P(\rho, x, t) \} \\ &\quad - \partial_x \{ [c h(f) \rho - \lambda x] P(\rho, x, t) \} \\ &\quad + \frac{1}{2M} \partial_\rho^2 \{ [e \rho + \lambda x (1 - \rho)] P(\rho, x, t) \} \\ &\quad + \frac{1}{2M} \partial_x^2 \{ [c h(f) \rho + (\lambda + 2\mathcal{D}) x] P(\rho, x, t) \} \\ &\quad - \frac{1}{M} \partial_x \partial_\rho \{ [\lambda x (1 - \rho) P(\rho, x, t)] \} \end{aligned} \quad (16)$$

as shown in Appendix A. Eq. (16) is a two-dimensional Fokker-Planck equation in the representative variables  $\rho$

and  $x$ . Hence, the corresponding Langevin equation can be straightforwardly derived, adopting the Itô prescription:

$$\begin{cases} \dot{x} = c h(f) \rho - \lambda x + \mathbb{B}^{xx} \eta_x \\ \dot{\rho} = \lambda x (1 - \rho) - e \rho + \mathbb{B}^{\rho\rho} \eta_\rho + \mathbb{B}^{\rho x} \eta_x \end{cases} \quad (17)$$

where the  $\vec{\eta} = (\eta_\rho, \eta_x)$  is uncorrelated white noise and the two-dimensional matrix  $\mathbb{B}$  is related to the Fokker-Planck diffusion matrix  $\hat{\mathbb{D}}$  of Eq. (16) through  $\hat{\mathbb{D}} = \mathbb{B}\mathbb{B}^T$ :

$$\hat{\mathbb{D}} = \frac{1}{M} \begin{pmatrix} c h(f) \rho + (\lambda + 2\mathcal{D}) x & -\lambda x (1 - \rho) \\ -\lambda x (1 - \rho) & e \rho + \lambda x (1 - \rho) \end{pmatrix}. \quad (18)$$

Since we are primarily interested in the persistence of settled populations, we further assume a separation of timescales in the dynamics of the explorers and the settled population. This results in a one-variable effective Langevin equation for the settled population (3), mirroring the deterministic generalization of the Hanski and Ovaskainen metapopulation model derived in [5]. The elimination of the variable  $x$  is, however, more involved than in the deterministic case, due to the presence of noise. We report the detailed calculations in Appendix A, resulting in the following one-dimensional Itô SDE:

$$\begin{aligned} \dot{\rho} &= [c h(f) (1 - \rho) - e] \rho \\ &\quad + \sqrt{\frac{1}{M} \rho \left[ \frac{c h(f)}{2(1+\mathcal{D}/\lambda)} (1 - \rho^2) + e \right]} \sigma(t) \end{aligned} \quad (19)$$

with  $\langle \sigma(t) \rangle = 0$ ,  $\langle \sigma(t) \sigma(s) \rangle = \delta(t - s)$ . To verify our derivation and assumptions, we numerically compare the



trajectories resulting from the stochastic QSS equation Eq. (19) with those obtained from a Gillespie simulation of the complete Master equation, which samples the exact microscopic dynamics of the model described in Eq. (1). As shown in Figure 1, we achieve a very good matching between the different trajectories in the survival regime. In the extinction regime, the mean densities are similar, but the Gillespie is slightly slower in extinction due to the absorbing boundary, which causes the explorer densities to always deviate from the quasi-stationary value. This suggests that the simplification methods considered up to this point are still able to reproduce the average behavior of the stochastic model under different parameters.

We can now exploit Eq. (19) to analyze the stochastic dynamics of the model. In particular, the mean-field settled population density  $\rho$  has domain  $(0, 1]$ , with an absorbing boundary at  $\rho = 0$ , that corresponds to population extinction.  $\rho = 1$  is instead a reflecting boundary, corresponding to the maximum number  $M$  of individuals that each patch can sustain. Deterministically, Eq. (19) yields an effective metapopulation capacity  $\lambda_M = h(f)$ , which still allows us to distinguish two regimes. When  $e/c > \lambda_M$ , the deterministic stationary solution is  $\rho_{st} = 0$ , corresponding to widespread extinction. If  $e/c < \lambda_M$  the stationary solution is instead given by  $\rho_{st} = \frac{1}{\lambda_M}(\lambda_M - \frac{e}{c})$ , which defines the survival regime in the deterministic mean-field model. However, due to the presence of noise, survival and extinction are no longer deterministic. In particular, if one solves the full stochastic Eq. (19) with the specified boundary conditions, it turns out that, even though the regime  $e/c < \lambda_M$  is still characterized by a long-lasting metastable state in which the population survives (see Figure 1), the only true stationary solution is  $\rho_{st} = 0$ . This reflects the well-known fact that phase transitions appear only in the thermodynamic limit of an infinite system size. Since the diffusion terms in the Fokker-Planck equations are inversely proportional to the local population size  $M$ , we anticipate that stochasticity will have a more pronounced impact on systems with a small carrying capacity. Indeed, as the population size decreases, the likelihood of a random fluctuation inducing extinction increases.

To investigate these effects, we need to compute the probabilities of survival and the time taken to reach extinction. These quantities provide comprehensive information about the impact of the absorbing boundary, and enable us to ascertain whether the regimes defined by the deterministic dynamics remain relevant when stochasticity is considered.

#### IV. SCALING PROPERTIES CLOSE TO THE TRANSITION

From the effective stochastic dynamics given by Eq. (19), we can investigate how the system size  $M$ , which is related to the amount of noise affecting the system, influences the survival probability.

Given an initial condition  $\rho$  at time  $t = 0$ , the survival probability is defined as the probability that the variable is still in its domain  $(0, 1]$  at time  $t$  [47]:

$$S(t|\rho, M) = \int_0^1 p(\rho', t|\rho, 0) d\rho', \quad (20)$$

where  $p(\rho', t|\rho, 0)$  is the solution of the FP equation related to Eq. (19), with the initial condition  $p(\rho', t = 0|\rho, 0) = \delta(\rho - \rho')$ . Related quantities are the mean exit time and its higher moments:

$$T_n(\rho, M) = \int_0^\infty p(t|\rho) t^n dt, \quad (21)$$

where  $p(t|\rho)$  is the probability distribution of extinction times, given the initial condition  $\rho$ . The latter probability distribution is connected to the survival probability through the relation  $p(t|\rho) = -\partial_t S(t|\rho)$  [47], which implies:

$$T_n(\rho, M) = \int_0^\infty t^{n-1} S(t|\rho, M) dt. \quad (22)$$

To investigate how the survival probability changes with the carrying capacity, we simulate the dynamics of the mean-field QSS stochastic differential equation corresponding to Eq. (19) for various values of  $M$ , using the Euler-Maruyama algorithm, with a total of  $10^7$  realizations. Figure 2a shows the numerical survival probability curves, with the system set at the boundary between the two regimes identified in the deterministic limit, i.e.  $e/c \equiv \lambda_M$ . We observe that the survival probability curves appear to exhibit a power-law behavior.

Hence, we adopt a typical finite-size scaling ansatz for the survival probability:

$$S(t|\rho, M) \propto \frac{1}{t^\alpha} \mathcal{F}_\rho(t M^\phi). \quad (23)$$

This corresponds to assuming that, close to the critical point, the survival probability is a generalized homogeneous function of time  $t$  and system size  $M$ . The scaling function  $\mathcal{F}_\rho$  depends on  $t$  and  $M$  only through their combination  $t M^\phi$ , and the exponents  $\phi$  and  $\alpha$  are expected to be independent of the details of the system. Plugging our ansatz (23) into Eq. (22) yields:

$$T_n(\rho, M) = \int_0^\infty \mathcal{F}_\rho(t M^\phi) t^{n-\alpha-1} dt = M^{-\phi(n-\alpha)} C_{n,\alpha}(\rho). \quad (24)$$

Notice that, by taking the ratio of two consecutive moments - as detailed in Appendix C 2 - we obtain:

$$\frac{\langle T^{n+1} \rangle}{\langle T^n \rangle} = \frac{C_{n+1,\alpha}(\rho)}{C_{n,\alpha}(\rho)} M^{-\phi} \quad (25)$$

where  $C_{n,\alpha}(\rho)$  depend only on the initial condition  $\rho$ . We can exploit the above relations to numerically verify

whether the finite-size scaling ansatz is correct and obtain a preliminary numerical estimate of the scaling exponents  $\alpha$  and  $\phi$ . By extracting the time to extinction from each realization of the simulation and fitting the moments' ratios as in Eq. (25), we can directly obtain the value of  $\phi$  and subsequently estimate  $\alpha$  from Eq. (24):

$$\phi = -0.506 \pm 0.002, \quad \alpha = -0.005 \pm 0.003. \quad (26)$$

Further details on the numerical derivation are provided in Appendix B. Ultimately, Figure 2b shows the collapse of the survival probability curves rescaled according to the numerical exponents in Eq. (26), which confirms our scaling hypothesis given in Eq. (23).

However, obtaining the scaling behavior of our system away from criticality presents more challenges: indeed, choosing a suitable scaling ansatz is not straightforward in this case. For this reason, we will adopt a more rigorous approach and analytically derive the scaling form of the moments of extinction time directly from the effective stochastic equation (24). This method yields the exact values of the scaling exponents even when the system is not poised at the critical point.

### A. First and second moments of exit time

We set  $T \equiv T_1$  and analytically investigate the scaling behavior of  $T_n$  with the carrying capacity  $M$ . We rely on the following differential equations, derived from the backward Fokker-Planck equations for the survival probability [47]:

$$A(\rho) \partial_\rho T(\rho) + \frac{1}{2} D(\rho) \partial_\rho^2 T(\rho) = -1 \quad (27)$$

$$A(\rho) \partial_\rho T_n(\rho) + \frac{1}{2} D(\rho) \partial_\rho^2 T_n(\rho) = -n T_{n-1}(\rho) \quad (28)$$

where  $A(\rho)$  and  $D(\rho)$  are the drift and diffusion coefficients of Eq. (19), respectively, and  $\rho$  is the initial condition of the settled population density at time  $t = 0$ .

We consider a setting in which the system is close to criticality and define the deviation from the critical point ( $e/c = \lambda_M$ ) through the parameter:

$$\Delta := \frac{1}{\lambda_M} \left( \lambda_M - \frac{e}{c} \right) = \frac{\epsilon}{\lambda_M}, \quad |\epsilon| \ll 1 \quad (29)$$

where  $\lambda_M = h(f)$ , as resulting from the deterministic part of the effective quasi-stationary Fokker-Planck Eq. (19). As shown in Appendix C1, by rescaling  $\rho \rightarrow \hat{\rho} = \rho \sqrt{M}$ ,  $T \rightarrow \hat{T} = \frac{\lambda_M c}{\sqrt{M}} T$  and  $\Delta \rightarrow \hat{\Delta} = \Delta \sqrt{M}$ , the equation for the first moment of exit time Eq. (27) becomes:

$$\left( \hat{\Delta} - \hat{\rho} \right) \hat{\rho} \partial_{\hat{\rho}} \hat{T} + \frac{\chi}{4} \hat{\rho} \partial_{\hat{\rho}}^2 \hat{T} = -1 \quad (30)$$

in the limit of large system size  $M$ . We have defined  $\chi := 3 + 2D/(\lambda \lambda_M)$ , which we treat as a fixed constant

in the following. Since Eq. (30) is independent of  $M$ , the rescaled extinction time  $\hat{T}$  is expected to be a function of the rescaled initial density  $\hat{\rho}$  and the rescaled distance from the critical point  $\hat{\Delta}$  alone. This implies that, in the limit of large  $M$ ,  $T$  has the scaling form:

$$T(\rho, \Delta, M) \propto \sqrt{M} \hat{T} \left( \sqrt{M} \rho, \sqrt{M} \Delta \right) \quad (31)$$

meaning it is a homogeneous function of  $\rho$  and  $\Delta$ . The solution of Eq. (30), with boundary conditions  $\hat{T}(0) = 0$ ,  $\partial_{\hat{\rho}} \hat{T}(\hat{\rho})|_{\hat{\rho}=\sqrt{M}} = 0$ , is given by the integral Eq. (C7), which can be evaluated analytically at criticality ( $\hat{\Delta}=0$ ) and numerically elsewhere.

To test our analytical predictions, we simulate the mean-field QSS SDE over  $10^5$  realizations, varying the distance from the critical point  $\Delta$ , the initial condition in the settled population density  $\rho$ , and the system size  $M$ . As shown in Figure 3a, the simulated points distribute within a volume in the three-dimensional space defined by  $\Delta$ ,  $\rho$ , and  $T$ . Upon rescaling the axes with  $M$  according to Eq. (31), the points collapse onto a single well-defined surface that encompasses different initial conditions and distances from criticality, consistently with the numerical evaluation of the analytically derived average extinction time (Eq. (C7)). We can now apply the same procedure to the equation for the second moment of the exit time, obtained by substituting  $n = 2$  into Eq. (28). The same analysis yields the following scaling expression:

$$T_2(\rho, \Delta, M) \propto M \hat{T}_2 \left( \sqrt{M} \rho, \sqrt{M} \Delta \right). \quad (32)$$

Figure 4 shows that rescaling the surfaces obtained from simulation data according to Eq. (32) leads to the collapse of these surfaces. We present further details of the derivation, along with an explicit analytical solution of the differential equation for  $T_2$ , in Appendix C1.

### B. Survival probability

Having found  $\langle T \rangle \propto \sqrt{M}$  (Eq. (31)) and  $\langle T^2 \rangle \propto M$  (Eq. (32)), we can determine the scaling of the survival probability at criticality ( $\Delta = 0$ ). The  $\phi$  exponent is obtained from Eq. (25):

$$\frac{\langle T^2 \rangle}{\langle T \rangle} \propto \sqrt{M} \Rightarrow \phi \equiv -\frac{1}{2}, \quad (33)$$

Subsequently, we can calculate the  $\alpha$  exponent (24) as

$$\langle T \rangle \propto M^{-\phi(1-\alpha)} \Rightarrow \alpha = 0 \quad (34)$$

which yields the following scaling form:

$$S(t|M) \propto f(t M^{-\frac{1}{2}}). \quad (35)$$

It is worth noting that the scaling exponents derived analytically and the ones obtained numerically reported in Eq. (26) agree remarkably well.)

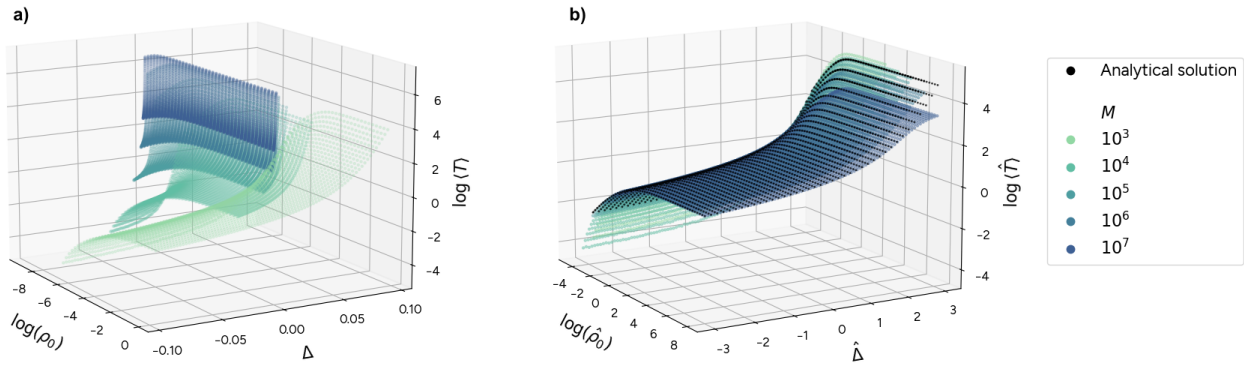


**FIG. 3.** First moment of exit time  $\langle T \rangle$  versus initial condition  $\rho_0$  and deviation from criticality  $\Delta$  for different values of the local carrying capacity  $M$ . **a)** not rescaled. **b)** rescaled according to Eq. (31). The black dots indicate the analytical solution Eq. (C7). Averages are obtained from  $10^5$  numerical realisations of the MF QSS dynamics in Eq. (19).

The technique we employed to analyze moments of extinction time can also be replicated for the survival probability. The starting point is once more the backward Fokker-Planck equation for the survival probability [47]:

$$\partial_t S = A(\rho) \partial_\rho S + \frac{1}{2} D(\rho) \partial_\rho^2 S. \quad (36)$$

Since Eq. (36) involves a time derivative, it is necessary to rescale both the initial condition and the time,

$$\rho \rightarrow \hat{\rho} = \rho M^\gamma \quad t \rightarrow \hat{t} = t \lambda_M c M^\phi. \quad (37)$$

After setting  $\phi = -\frac{1}{2}$  and  $\gamma = \frac{1}{2}$ , the following size-independent equation is attained:

$$\partial_{\hat{t}} S = (\hat{\Delta} - \hat{\rho}) \hat{\rho} \partial_{\hat{\rho}} S + \frac{\chi}{4} \hat{\rho} \partial_{\hat{\rho}}^2 S \quad (38)$$

from which we derive (see Appendix C2 for more details):

$$S = S \left( \frac{t}{\sqrt{M}}, \sqrt{M} \rho, \sqrt{M} \Delta \right). \quad (39)$$

This scaling is consistent with our previous findings regarding the first and second moments of extinction time, but it now offers a more general form that relates to the entire distribution of extinction times rather than its specific moments. By fixing the distance from the critical point  $\Delta = 0$  and the initial condition  $\rho$ , we recover our result in Eq. (35).

The scaling relations of survival probability at criticality and moments of extinction time away from criticality can be summarized as follows:

$$\begin{aligned} S(t|M) &= t^{-\alpha} \hat{S}(tM^\phi) \\ T_1(\rho, \Delta, M) &= M^\beta \hat{T}_1(\rho M^\gamma, \Delta M^\eta) \\ T_2(\rho, \Delta, M) &= M^\delta \hat{T}_2(\rho M^\gamma, \Delta M^\eta) \end{aligned} \quad (40)$$

with the exponents connected through the scaling relations

$$\beta = -\phi(1 - \alpha), \quad \delta = -\phi(2 - \alpha) \quad (41)$$

and their numerical values are reported in Table I.

$\alpha$	$\phi$	$\gamma$	$\eta$	$\beta$	$\delta$
0	$-\frac{1}{2}$	$\frac{1}{2}$	$\frac{1}{2}$	$\frac{1}{2}$	1

**TAB. I.** Scaling exponents characterizing the survival probability  $S$  and the first and second moments of the exit time,  $T_1$  and  $T_2$  in the vicinity of the critical point.

## V. CONCLUSIONS

In this work, we extended the traditional metapopulation framework to incorporate stochasticity, with the aim of investigating its impact on metapopulation persistence. We focused on understanding the role of finite carrying capacity in the subpopulation size, which is directly associated with the strength of demographic fluctuations. In doing so, we were able to quantitatively address the dynamics of finite metapopulations and study their stochastic evolution.

Our results suggest that, for a simple colonization-death dynamics in homogeneous landscapes governed by mean-field dispersal networks, the introduction of stochasticity does not lead to strong deviations from the deterministic population dynamics. Yet, we uncovered the unexpected appearance of an absorbing boundary even in the regime in which the population would deterministically survive. Hence, the stochastic metapopulation always faces eventual extinction due to the finite carrying capacity. Additionally, we have found strong consistency with finite-size scaling predictions, as evidenced by the collapse of the survival probability and extinction time moments curves. The scaling exponents governing this collapse have been analytically derived from the backward Fokker-Planck equation of the model (Table I) as well as verified through numerical simula-



tions. These results provide a baseline expectation for further studies into stochastic metapopulation models. The bottom-up derivation of the Fokker-Planck equation and the effective Langevin equation present immediate numerical applications beyond mean-field networks to incorporate interesting topological factors which were omitted for the sake of analytical simplicity. Changes in the scaling exponents will not only provide possible connections to universality classes but also connect network topology and average time to extinction induced by demographic stochasticity.

Natural ecosystems present numerous complexities beyond the simplified scenario considered here. For instance, heterogeneity in local parameters can foster multispecies coexistence through localization, as demonstrated in deterministic metacommunity models [27]. Non-trivial network topologies are also expected to play an important role in shaping the fluctuations of the metapopulation density. For instance, dendritic river networks affect ecological dynamics [50], and the spatial structure of the diffusion network can influence the probability of fixation of a mutation in stochastic metapopulation models of microbial communities [51, 52]. Similarly, environmental co-factors, such as wildfires influencing forest dynamics [53], and stochastic or time-varying dispersal [54–56], can significantly alter the impact of demographic stochasticity. Our effective SDE provides a framework to capture these effects by appropriately modeling boundary conditions [57, 58]. Furthermore, increased distances from criticality or comparable timescales of explorer and settled population dynamics - as observed in seascape ecology - are likely to shape both survival and extinction time distributions. In the survival regime, above the deterministic critical threshold, the existence of long metastable states also facilitates the study of the response to environmental perturbations on both dynamics of population and its persistence [59]. Future studies addressing these factors will enhance our understanding of the processes that support or undermine the persistence of spatially structured populations. Overall, our results provide a foundation for integrating more complex and realistic effects into stochastic metapopulation models. By refining microscopic processes and dispersal network topology, these extensions will further elucidate the critical role of stochasticity in the survival of spatially structured populations.

## ACKNOWLEDGMENTS

A.D. and D.B. were supported by the Italian Ministry of University and Research (project funded by the European Union - Next Generation EU: “PNRR Missione 4 Componente 2, “Dalla ricerca all’impresa”, Investimento 1.4, Progetto CN00000033”). G.N. acknowledges funding provided by the Swiss National Science Foundation through its Grant CRSII5\_186422. P.P. was funded by NCCR Microbiomes Grant 51NF40\_180575 from the

Swiss National Science Foundation. The authors thank Amos Maritan and Sandro Azaele for very helpful discussions and important comments on the paper.

## Appendix A: Mean-field model

Let us consider a complete network (whose adjacency matrix is  $\mathcal{A}_{ij} = \mathcal{A}(1 - \delta_{ij})$  with  $\mathcal{A} = 1/N$ ) and assume patch homogeneity:  $c_i = c \forall i$ ,  $e_i = e \forall i$ . Under these hypotheses, the drift Eq. (11) and diffusion Eq. (12) coefficients of the Fokker-Planck equation become:

$$\begin{aligned} A_i^p &= \lambda x_i(1 - \rho_i) - e \rho_i \\ A_i^x &= \frac{1}{N} \sum_j \left( \mathcal{D}x_j + ch(f)\rho_j \right) - \frac{1}{N} ch(f)\rho_i - (\mathcal{D} + \lambda)x_i \\ \mathbb{D}_{ij}^{\rho\rho} &= \frac{1}{M} [e\rho_i + \lambda x_i(1 - \rho_i)] \delta_{ij} \\ \mathbb{D}_{ij}^{\rho x} &= \mathbb{D}_{ij}^{x\rho} = -\frac{1}{M} \lambda x_i(1 - \rho_i) \delta_{ij} \\ \mathbb{D}_{ij}^{xx} &= \frac{1}{M} \left[ \frac{1}{N} \sum_k \left( \mathcal{D}x_k + ch(f)\rho_k \right) + \right. \\ &\quad \left. + (\mathcal{D} + \lambda)x_i - \frac{1}{N} ch(f)\rho_i \right] \delta_{ij} - \frac{2}{MN} \mathcal{D}x_i(1 - \delta_{ij}) \end{aligned} \quad (\text{A1})$$

After applying the marginalization procedure described in Eq. (14) and (15), we obtain a two-dimensional Fokker-Planck equation in the representative variables  $(x, \rho)$ , as reported in Eq. (16). The drift vector and diffusion matrix are given by:

$$\begin{aligned} \vec{A} &= \begin{pmatrix} \lambda x(1 - \rho) - e\rho \\ ch(f)\rho - \lambda x \end{pmatrix} \\ \hat{\mathbb{D}} &= \frac{1}{M} \begin{pmatrix} ch(f)\rho + (\lambda + 2\mathcal{D})x & -\lambda x(1 - \rho) \\ -\lambda x(1 - \rho) & e\rho + \lambda x(1 - \rho) \end{pmatrix} \end{aligned} \quad (\text{A2})$$

The corresponding Langevin equation in Eq. (17) can be derived by imposing  $\mathbb{B}\mathbb{B}^T = \hat{\mathbb{D}}$  for  $\mathbb{B}$  in the form:

$$\mathbb{B} = \begin{pmatrix} \mathbb{B}^{xx} & \mathbb{B}^{x\rho} \\ 0 & \mathbb{B}^{\rho x} \end{pmatrix} \quad (\text{A3})$$

which yields:

$$\begin{aligned} \mathbb{B}^{xx} &= \frac{1}{\sqrt{M}} \sqrt{ch(f)\rho + (\lambda + 2\mathcal{D})x} \\ \mathbb{B}^{\rho x} &= -\frac{1}{\sqrt{M}} \frac{\lambda x(1 - \rho)}{\sqrt{ch(f)\rho + (\lambda + 2\mathcal{D})x}} \\ \mathbb{B}^{x\rho} &= \frac{1}{\sqrt{M}} \sqrt{e\rho + \lambda x(1 - \rho) - \frac{\lambda^2 x^2 (1 - \rho)^2}{ch(f)\rho + (\lambda + 2\mathcal{D})x}} \end{aligned} \quad (\text{A4})$$

We can now derive the effective equation in the settled population density, by assuming a separation of timescales in the settled and explorer population’s dynamics. Consider Eq. (17) and let  $\bar{x}$  be the stationary value of  $x$  such that  $\dot{x} = 0$ :

$$\bar{x} = \frac{ch(f)\rho}{\lambda}, \quad \eta_x \equiv 0 \quad (\text{A5})$$

If we condition  $\rho$  on  $x$  being fixed at  $\bar{x}$ , we obtain:

$$\dot{\rho} = c h(f) \rho(1 - \rho) - e \rho + B^{\rho\rho} \Big|_{x=\bar{x}} \eta_\rho \quad (\text{A6})$$

which yields the quasi-stationary stochastic Eq. (19).

### Appendix B: Numerical scaling exponents for the survival probability

Given the finite size scaling assumption Eq. (23) for the survival probability's time dependence, we can express the  $n$ -th moment of exit time as:

$$\begin{aligned} \langle T^n(\rho, M) \rangle &= - \int_0^\infty \partial_t S(t|\rho, M) t^n dt \\ &= \int_0^\infty S(t|\rho, M) t^{n-1} dt \end{aligned} \quad (\text{B1})$$

by substituting the scaling hypothesis Eq. (23) we obtain:

$$\begin{aligned} \langle T^n(\rho, M) \rangle &\propto \int_0^\infty \mathcal{F}_\rho(tM^\phi) t^{n-\alpha-1} dt \\ &= M^{-\phi(n-\alpha)} \int_0^\infty \mathcal{F}_\rho(z) z^{n-\alpha-1} dz \\ &= M^{-\phi(n-\alpha)} C_{n,\alpha}(\rho) \end{aligned} \quad (\text{B2})$$

and

$$\frac{\langle T^{n+1} \rangle}{\langle T^n \rangle} = \frac{C_{n+1,\alpha}(\rho)}{C_{n,\alpha}(\rho)} M^{-\phi} \quad (\text{B3})$$

where the explicit dependence on the initial condition  $\rho$  is included in the  $C_{n,\alpha}$  coefficients. The above Eq. (B3) allows to numerically estimate the  $\phi$  exponent. To achieve this, we simulate  $10^7$  realizations of the MF QSS dynamics given by Eq. (19) and we compute the moments of extinction time. Specifically, we select the moments of order  $n$  ranging from 1 to 8, and consider 20 values for  $M$ , spanning from  $10^3$  to  $10^7$ . For any two consecutive moments, we fit the logarithm of  $\frac{\langle T^{n+1} \rangle}{\langle T^n \rangle}$  as a function of  $\log(M)$ . In principle, this yields 7 parallel lines. The average of the obtained slopes provides therefore our estimate for  $\phi$ . The error is taken to be the standard deviation of the slopes.

Once  $\phi$  is determined, we can exploit Eq. (B2) to estimate  $\alpha$ . In particular, we now fit the logarithm of  $\langle T^n \rangle$  versus  $\log(M)$ , and  $\alpha$  is obtained from the slope  $m$  of the fitted lines, namely:  $m = -\phi(n - \alpha)$ . We consider the standard deviation of  $\alpha$  as its error.

However, the estimates of  $\phi$  and  $\alpha$  are highly influenced from the values of  $M$  considered, the number of realizations of the dynamics and the order of the moments used for the fitting. In particular, higher values of  $M$  and a larger number of realizations provide more rigorous estimates, as confirmed by deviations from the linearly expected behavior becoming less pronounced. The errors computed as standard deviations are therefore not fully representative of the true uncertainty in the estimates, as they do not account for these factors, which introduce additional variability.

### Appendix C: Scaling Analysis

Let us express the mean-field QSS stochastic equation Eq. (19) in the more convenient Fokker-Planck formalism:

$$\partial_t P(\rho, t) = -\partial_\rho [A(\rho)P(\rho, t)] + \frac{1}{2} \partial_\rho^2 [D(\rho)P(\rho, t)] \quad (\text{C1})$$

This is a one-dimensional time-homogeneous FP equation. The domain of  $\rho$  is given by the interval  $(0, 1]$ , with  $\rho = 0$  absorbing boundary and  $\rho = 1$  reflecting boundary, as seen in Section III B. Therefore, the definition of survival probability given in Eq. (20) implies that it obeys the boundary conditions  $S(0, t) = 0$ ,  $\partial_\rho S(\rho, t)|_{\rho=1} = 0$ . Through Eq. (22) we similarly find  $T_n(0, t) = 0$ ,  $\partial_\rho T_n(\rho, t)|_{\rho=1} = 0$  for the  $n$ -th moment of extinction time.

For the upcoming calculations, we rewrite the drift and diffusion coefficients of the QSS mean-field Fokker-Planck equation in terms of the parameter  $\Delta$  Eq. (29), which quantifies the deviation from criticality:

$$\begin{aligned} A(\rho, M, \Delta) &= \lambda_M c (\Delta - \rho) \rho \\ D(\rho, M, \Delta) &= \frac{\lambda_M c}{2M} \left( 3 - \rho^2 - 2\Delta + \frac{2D}{\lambda \lambda_M} \right) \rho \end{aligned} \quad (\text{C2})$$

#### 1. First and second moments of exit time

Consider Eq. (27) for the first moment of exit time:

$$\begin{aligned} (\Delta - \rho) \rho \partial_\rho T + \\ + \frac{1}{4M} \left( 3 - \rho^2 - 2\Delta + \frac{2D}{\lambda \lambda_M} \right) \rho \partial_\rho^2 T = -\frac{1}{\lambda_M c} \end{aligned} \quad (\text{C3})$$

In order to achieve a common scaling of the LHS with the system size  $M$ , it is convenient to rescale  $\rho \rightarrow \hat{\rho} = \rho \sqrt{M}$ ,  $T \rightarrow \hat{T} = \frac{\lambda_M c}{\sqrt{M}} T$  and  $\Delta \rightarrow \hat{\Delta} = \Delta \sqrt{M}$

$$\begin{aligned} (\hat{\Delta} - \hat{\rho}) \hat{\rho} \partial_{\hat{\rho}} \hat{T} + \\ + \frac{1}{4} \left( \chi - \frac{\hat{\rho}^2}{M} - 2 \frac{\hat{\Delta}}{\sqrt{M}} \right) \hat{\rho} \partial_{\hat{\rho}}^2 \hat{T} = -1 \end{aligned} \quad (\text{C4})$$

where we define  $\chi := 3 + 2D/(\lambda \lambda_M)$ , which we treat as a fixed constant in the following. In the limit of large system size  $M$ , the terms  $\frac{\hat{\rho}^2}{M}$ ,  $\frac{\hat{\Delta}}{\sqrt{M}}$  can be neglected, yielding the following equation:

$$\left( \hat{\Delta} - \hat{\rho} \right) \hat{\rho} \partial_{\hat{\rho}} \hat{T} + \frac{\chi}{4} \hat{\rho} \partial_{\hat{\rho}}^2 \hat{T} = -1 \quad (\text{C5})$$

which is independent of  $M$ . Therefore, for large  $M$  the first exit time scales as:

$$T(\rho, \Delta, M) \propto \sqrt{M} \hat{T} \left( \sqrt{M} \rho, \sqrt{M} \Delta \right) \quad (\text{C6})$$

From the above expression we observe that the rescaled first exit time should depend only on the rescaled initial density  $\hat{\rho} = \sqrt{M} \rho$  and the rescaled distance from

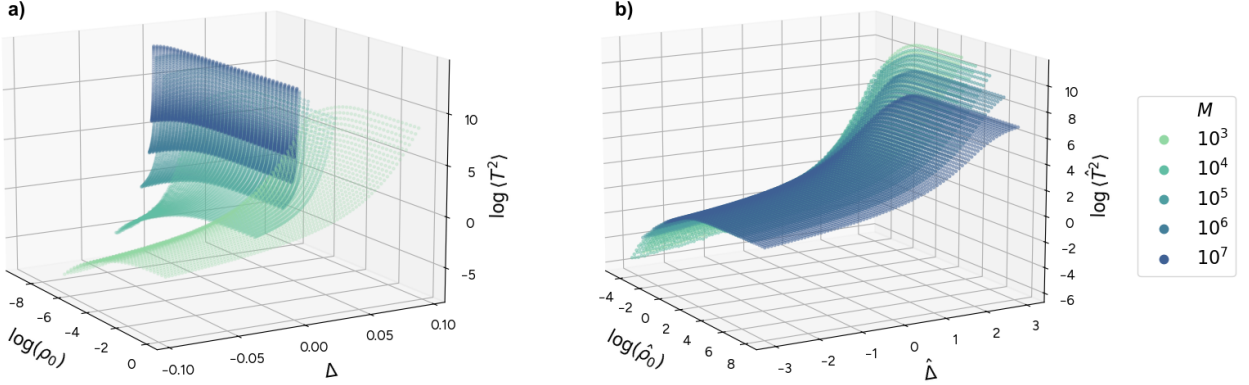


**FIG. 4.** Second moment of exit time  $\langle T^2 \rangle$  versus initial condition  $\rho_0$  and deviation from criticality  $\Delta$  for different values of the local carrying capacity  $M$ . **a)** not rescaled. **b)** rescaled according to Eq. (32). Averages are obtained from  $10^5$  numerical realizations of the MF QSS dynamics in Eq. (19).

the critical point  $\hat{\Delta} = \sqrt{M}\Delta$ . The solution of Eq. (C5) with  $\hat{\rho} \in (0, \sqrt{M}]$  and boundary conditions  $\hat{T}(0) = 0$ ,  $\partial_{\hat{\rho}}\hat{T}(\hat{\rho})|_{\hat{\rho}=\sqrt{M}} = 0$  is given by the integral:

$$\begin{aligned} \hat{T}(\hat{\rho}, \hat{\Delta}) &= \frac{4}{\chi} \int_0^{\hat{\rho}} dx e^{-G(x, \hat{\Delta})} \int_x^{\sqrt{M}} dy \frac{e^{G(y, \hat{\Delta})}}{y} \\ G(\hat{\rho}, \hat{\Delta}) &= \frac{4}{\chi} \int_{\sqrt{M}}^{\hat{\rho}} dx (\hat{\Delta} - x) \\ &= \frac{2}{\chi} \left[ 2\hat{\Delta}(x - \sqrt{M}) + M - x^2 \right] \end{aligned} \quad (\text{C7})$$

In particular, in the simple case of  $\hat{\Delta} = 0$  (criticality) the integral Eq. (C7) can be calculated analytically:

$$\begin{aligned} \hat{T}(\hat{\rho}) &= \frac{4}{\chi} \hat{\rho} {}_2F_2 \left( \frac{1}{2}, 1; \frac{3}{2}, \frac{3}{2}; -\frac{2}{\chi} \hat{\rho}^2 \right) + \\ &+ \sqrt{\frac{\pi}{2\chi}} \operatorname{erfi} \left( \sqrt{\frac{2}{\chi}} \hat{\rho} \right) \left( \operatorname{Ei} \left( -\frac{2}{\chi} M \right) - \operatorname{Ei} \left( -\frac{2}{\chi} \hat{\rho}^2 \right) \right) \end{aligned} \quad (\text{C8})$$

where  $\operatorname{erfi}(x)$  is the imaginary error function,  $\operatorname{Ei}(x)$  is the exponential integral function and  ${}_pF_q(\{a_1, \dots, a_p\}; \{b_1, \dots, b_q\}; z)$  is the generalized hypergeometric function.

Consider now the second moment of extinction time ( $n = 2$  in Eq. (28)):

$$(\Delta - \rho) \rho \partial_{\rho} T_2 + \frac{1}{4M} (\chi - \rho^2 - 2\Delta) \rho \partial_{\rho}^2 T_2 = -2 \frac{T_1}{\lambda_M c} \quad (\text{C9})$$

where  $T_1$  is the first moment, which scales according to Eq. (31). Rescaling  $T_2 \rightarrow \hat{T}_2 = \frac{(\lambda_M c)^2}{2M} T_2$  and neglecting terms  $\sim \mathcal{O}(\frac{1}{\sqrt{M}})$ , Eq. (C9) becomes:

$$(\hat{\Delta} - \hat{\rho}) \hat{\rho} \partial_{\hat{\rho}} \hat{T}_2 + \frac{\chi}{4} \hat{\rho} \partial_{\hat{\rho}}^2 \hat{T}_2 = -\hat{T} \quad (\text{C10})$$

which shows that the second moment of exit time scales as:

$$T_2(\rho, \Delta, M) \propto M \hat{T}_2 \left( \sqrt{M}\rho, \sqrt{M}\Delta \right) \quad (\text{C11})$$

The analytical solution is given by:

$$\hat{T}_2(\hat{\rho}, \hat{\Delta}) = \frac{4}{\chi} \int_0^{\hat{\rho}} dx e^{-G(x, \hat{\Delta})} \int_x^{\sqrt{M}} dy \frac{\hat{T}(y, \hat{\Delta})}{y} e^{G(y, \hat{\Delta})} \quad (\text{C12})$$

with  $G(\hat{\rho}, \hat{\Delta})$  and  $\hat{T}(\hat{\rho}, \hat{\Delta})$  defined in Eq. (C7). As done for the mean extinction time, we numerically calculate the second moment of extinction time by simulating  $10^5$  realizations of the mean-field QSS dynamics given in Eq. (19), using the Euler-Maruyama algorithm (cite). By applying the proper rescaling, we obtain again a good collapse of the second moment of extinction time as a function of the distance from the critical point  $\Delta$ , the initial condition  $\rho$  and the system size  $M$ . The collapse is shown in Figure 4.

## 2. Survival probability

Starting from Eq. (36), we apply the rescaling procedure:

$$t \rightarrow \hat{t} = t \lambda_M c M^{\nu} \quad \rho \rightarrow \hat{\rho} = \rho M^{\gamma} \quad (\text{C13})$$

which yields:

$$\begin{aligned} M^{\nu} \partial_{\hat{t}} S &= M^{-\gamma} (\Delta M^{\gamma} - \hat{\rho}) \hat{\rho} \partial_{\hat{\rho}} S \\ &+ \frac{1}{4} M^{\gamma-1} \left( \chi - \frac{\hat{\rho}^2}{M^{2\gamma}} - 2\Delta \right) \hat{\rho} \partial_{\hat{\rho}}^2 S \end{aligned} \quad (\text{C14})$$

It is then convenient to choose  $\nu, \gamma$  such that  $\nu = -\gamma = \gamma - 1 \rightarrow \gamma = \frac{1}{2}, \nu = -\frac{1}{2}$

$$\partial_t S = (\hat{\Delta} - \hat{\rho})\hat{\rho} \partial_{\hat{\rho}} S + \frac{1}{4} \left( \chi - \frac{\hat{\rho}^2}{M} - 2 \frac{\hat{\Delta}}{\sqrt{M}} \right) \hat{\rho} \partial_{\hat{\rho}^2} S \quad (\text{C15})$$

where  $\hat{\Delta} = \Delta \sqrt{M}$ . Neglecting  $\mathcal{O}(\frac{1}{\sqrt{M}})$  terms:

$$\partial_t S = (\hat{\Delta} - \hat{\rho})\hat{\rho} \partial_{\hat{\rho}} S + \frac{\chi}{4} \hat{\rho} \partial_{\hat{\rho}^2} S \quad (\text{C16})$$

We deduce the following scaling behavior of the survival probability:

$$S(t, \rho, \Delta, M) = S \left( \frac{t}{\sqrt{M}}, \sqrt{M}\rho, \sqrt{M}\Delta \right) \quad (\text{C17})$$

which is consistent with the scaling of  $S$  determined through the previous approach.

- 
- [1] M. A. Leibold, M. Holyoak, N. Mouquet, P. Amarasekare, J. M. Chase, M. F. Hoopes, R. D. Holt, J. B. Shurin, R. Law, D. Tilman, *et al.*, *Ecology letters* **7**, 601 (2004).
- [2] I. Hanski, *Nature* **396**, 41 (1998).
- [3] I. Hanski, *Biological Journal of The Linnean Society* **42**, 17 (1991).
- [4] I. Hanski and O. Ovaskainen, *Theoretical population biology* **64**, 119 (2003).
- [5] G. Nicoletti, P. Padmanabha, S. Azaele, S. Suweis, A. Rinaldo, and A. Maritan, *Proceedings of the National Academy of Sciences* **120**, e2311548120 (2023), <https://www.pnas.org/doi/pdf/10.1073/pnas.2311548120>.
- [6] I. Hanski, *Oikos*, 390 (1998).
- [7] S. Wang, B. Haegeman, and M. Loreau, *PeerJ* **3**, e1295 (2015).
- [8] M. Loreau, N. Mouquet, and R. D. Holt, *Ecology Letters* **6**, 673 (2003).
- [9] M. Loreau, N. Mouquet, and A. Gonzalez, *Proceedings of the National Academy of Sciences* **100**, 12765 (2003).
- [10] J. N. Marleau, F. Guichard, and M. Loreau, *Proceedings of the Royal Society B: Biological Sciences* **281**, 20132094 (2014).
- [11] R. Levins, *Bulletin of the Entomological Society of America* **15**, 237 (1969), <https://academic.oup.com/ae/article-pdf/15/3/237/18805526/besa15-0237.pdf>.
- [12] M. Holyoak, *American Naturalist* **156**, 378 (2000).
- [13] B. Rayfield, C. Baines, L. Gilarranz, and A. Gonzalez, *Proceedings of the National Academy of Sciences* **120** (2023).
- [14] M. Bevanda, E. Fronhofer, M. Heurich, J. Müller, and B. Reineking, *Ecosphere* **6**, 195 (2015).
- [15] P. Staddon, Z. Lindo, P. Crittenden, F. Gilbert, and A. Gonzalez, *Ecology letters* **13**, 543 (2010).
- [16] P. Arancibia and P. Morin, *Journal of Animal Ecology* **91** (2021).
- [17] I. Hanski and O. Ovaskainen, *Nature* **404**, 755 (2000).
- [18] I. Hanski, *Metapopulation Ecology* (Oxford University Press, 1999).
- [19] O. Ovaskainen, K. Sato, J. Bascompte, and I. Hanski, *Journal of Theoretical Biology* **215**, 95 (2002).
- [20] O. Ovaskainen and I. Hanski, in *Ecology, genetics and evolution of metapopulations* (Elsevier, 2004) pp. 73–103.
- [21] P. Marquet, R. Q. ones, S. Abades, F. Labra, M. Tognelli, M. Arim, and M. Rivadeneira, *The Journal of Experimental Biology* **208**, 1749 (2005).
- [22] J. M. Montoya, S. L. Pimm, and R. V. Solé, *Nature* **442**, 259 (2006).
- [23] M.-J. Fortin, M. R. Dale, and C. Brimacombe, *Proceedings of the Royal Society B* **288**, 20201889 (2021).
- [24] J. W. White, L. W. Botsford, A. Hastings, and J. L. Largier, *Marine Ecology Progress Series* **398**, 49 (2010).
- [25] M. D. Holland and A. Hastings, *Nature* **456**, 792 (2008).
- [26] L. J. Gilarranz and J. Bascompte, *Journal of Theoretical Biology* **297**, 11 (2012).
- [27] P. Padmanabha, G. Nicoletti, D. Bernardi, S. Suweis, S. Azaele, A. Rinaldo, and A. Maritan, *Proceedings of the National Academy of Sciences* **121**, e2410932121 (2024).
- [28] J. Grilli, G. Barabás, and S. Allesina, *PLoS Computational Biology* **11**, e1004251 (2015).
- [29] M. B. Bonsall and A. Hastings, *Journal of Animal Ecology* **73**, 1043 (2004).
- [30] M. Mangel and C. Tier, *Theoretical Population Biology* **44**, 1 (1993).
- [31] Y. M. Lai, J. Newby, and P. C. Bressloff, *Physical review letters* **107**, 118102 (2011).
- [32] S. Engen, R. Lande, and B.-E. Saether, *Ecology* **84**, 2378 (2003).
- [33] I. Hanski, *Journal of Animal Ecology* **63**, 151 (1994).
- [34] J. R. Day and H. P. Possingham, *Theoretical population biology* **48**, 333 (1995).
- [35] A. Moilanen, *Ecological modelling* **179**, 533 (2004).
- [36] J. VERBOOM, K. LANKESTER, and J. A. METZ, *Biological Journal of the Linnean Society* **42**, 39 (1991).
- [37] R. S. Etienne and J. A. Heesterbeek, *The American naturalist* **158(4)**, 389–407 (2001).
- [38] J. Ross, *Bulletin of mathematical biology* **68**, 417 (2006).
- [39] C. Sutherland, D. Elston, and X. Lambin, *Ecology* **95**, 3149 (2014).
- [40] Y. Tao, A. Hastings, K. D. Lafferty, I. Hanski, and O. Ovaskainen, *Proceedings of the National Academy of Sciences* **121**, e2303846121 (2024).
- [41] N. G. Van Kampen, *Stochastic processes in physics and chemistry*, Vol. 1 (Elsevier, 1992).
- [42] G. Nicoletti and D. M. Busiello, *Physical Review X* **14**, 021007 (2024).
- [43] G. Grinstein and M. A. Muñoz, in *Fourth Granada Lectures in Computational Physics: Proceedings of the 4th Granada Seminar on Computational Physics Held at Granada, Spain, 9–14 September 1996* (Springer, 1997) pp. 223–270.
- [44] M. A. Munoz, G. Grinstein, and Y. Tu, *Physical Review E* **56**, 5101 (1997).
- [45] M. E. Fisher, *Reports on Progress in Physics* **31**, 418 (1968).

- [46] F. Hahne, *Critical Phenomena: Proceedings of the Summer School Held at the University of Stellenbosch, South Africa, January 18-29, 1982*, Lecture Notes in physics. Springer (Springer-Verlag, 1983).
- [47] C. W. Gardiner *et al.*, *Handbook of stochastic methods*, Vol. 3 (springer Berlin, 1985).
- [48] D. T. Gillespie, *Journal of Computational Physics* **22**, 403 (1976).
- [49] N. Kampen, *Canadian Journal of Physics* **39**, 551 (2011).
- [50] F. Carrara, F. Altermatt, I. Rodriguez-Iturbe, and A. Rinaldo, Proceedings of the National Academy of Sciences **109**, 5761 (2012).
- [51] L. Marrec, I. Lamberti, and A.-F. Bitbol, *Physical Review Letters* **127**, 218102 (2021).
- [52] A. Abbara, L. Pagani, C. García-Pareja, and A.-F. Bitbol, *PLOS Computational Biology* **20**, 1 (2024).
- [53] G. Nicoletti, L. Saravia, F. Momo, A. Maritan, and S. Suweis, *Iscience* **26** (2023).
- [54] P. D. Williams and A. Hastings, *The American Naturalist* **182**, 271 (2013).
- [55] R. E. Snyder, C. B. Paris, and A. C. Vaz, *The American Naturalist* **184**, 523 (2014).
- [56] P. V. Martín, V. Domínguez-García, and M. A. Muñoz, *New Journal of Physics* **22**, 083014 (2020).
- [57] D. Bernardi and B. Lindner, *Physical Review Letters* **128**, 040601 (2022).
- [58] M. Su, D. Bernardi, and B. Lindner, *New Journal of Physics* **25**, 023033 (2023).
- [59] P. Padmanabha, S. Azaele, and A. Maritan, *New Journal of Physics* **25**, 113001 (2023).